ADVANCED FUNCTIONAL MATERIALS
www.afm-journal.de

Flexible $Nb_4C_3T_x$ Film with Large Interlayer Spacing for High-Performance Supercapacitors

Shuangshuang Zhao, Chaofan Chen, Xin Zhao, Xuefeng Chu, Fei Du, Gang Chen, Yury Gogotsi, Yu Gao,* and Yohan Dall'Agnese**

MXenes derived from 413 MAX phases are rarely studied but they have the potential to have superior electrical and mechanical properties thanks to a thicker monolayer (four layers of transition metal and three layers of carbon or nitrogen). In this paper, $Nb_4C_3T_x$ MXene nanosheets are delaminated and freestanding film with 1.77 nm interlayer spacing is obtained, which is larger than that of most previous MXenes. When $Nb_4C_3T_x$ freestanding films are tested as supercapacitors electrodes, $Nb_4C_3T_x$ shows high volumetric capacitance, 1075, 687, and 506 F cm^{-3} in 1 M H_2SO_4, 1 M KOH, and 1 M $MgSO_4$, respectively, at the scan rate of 5 mV s^{-1}. An in situ X-ray diffraction technique is used to study the structural changes during the electrochemical charging in 1 M H_2SO_4 and 1 M $MgSO_4$. There is almost no change in the 21 Å interlayer spacing during the cycling, because the space between the MXene layers is sufficient to accommodate the insertion and deinsertion of cations. This can lead to stable performance of $Nb_4C_3T_x$ MXene energy storage devices.

1. Introduction

The development of portable and wearable electronic devices has posed new challenges to clean energy storage. There are many ways to satisfy charging, such as rechargeable secondary batteries (lithium, sodium, potassium, etc.), fuel cells, various ion capacitors, etc. However, comparing with other reported energy storage devices, supercapacitors can carry out rapid charging and discharging to complete the energy supply, meeting customers' needs.[1] Supercapacitors mainly rely on two different ways to store energy: the adsorption of electrostatic charges on the surface of the electrode/electrolyte and the pseudocapacitance from the fast surface redox reaction.[2,3] Finding flexible materials with high volumetric performance suitable for supercapacitors has become an important target.

In the world of nanomaterials, 2D materials have become important candidates for energy storage due to their large specific surface area and good conductivity. Among them, the most noticeable are MXenes, which are etched from ternary transition metal carbonitrides. At present, there are more than 30 known MXene materials, with general chemical formula of $M_{n+1}X_nT_x$ where M is a transition metal, X is carbon and/or nitrogen, and T_x is surface termination (OH, O, F). MXenes such as Ti_2CT_x,[4] $Ti_3C_2T_x$,[5] V_2CT_x,[6] $Nb_4C_3T_x$,[7] Nb_2CT_x[8] are well known and show promise in the field of hydrogen storage,[9] photocatalysis,[10] solar cells,[11] sewage treatment,[12] and especially energy storage.[13] MXenes and their composites have shown excellent capacitance performance in supercapacitors. Taking $Ti_3C_2T_x$ as an example, previous reports show that the capacitance is up to 900 F cm^{-3} in 1 M H_2SO_4 and 1500 F cm^{-3} in 3 M H_2SO_4.[14,15] In 6 M KOH, it is 393 F cm^{-3} (d-Ti_3C_2/CNT) and 528 F cm^{-3} ($Ti_3C_2T_x$/PVA-KOH) in 1 M KOH;[16,17] in 1 M $MgSO_4$, it is about 280 F cm^{-3}.[18] Those values are higher compared to majority of other supercapacitor electrodes.

S. Zhao, C. Chen, X. Zhao, Prof. F. Du, Prof. G. Chen, Prof. Y. Gao
Key Laboratory of Physics and Technology for Advanced Batteries (Ministry of Education)
College of Physics
Jilin University
Changchun 130012, P. R. China
E-mail: yugao@jlu.edu.cn

S. Zhao, Prof. Y. Gogotsi
A. J. Drexel Nanomaterials Institute
and Department of Materials Science and Engineering
Drexel University
Philadelphia, PA 19104, USA
E-mail: gogotsi@drexel.edu

Prof. X. Chu
Comprehensive Energy Saving
School of Electrical and Electronic Information Engineering
Jilin Jianzhu University
Changchun 130118, P. R. China

Prof. G. Chen
State Key Laboratory of Superhard Materials
Jilin University
Changchun 130012, P. R. China

Dr. Y. Dall'Agnese
Institute for Materials Discovery
University College London
London WC1E 7JE, UK
E-mail: y.dallagnese@ucl.ac.uk

The ORCID identification number(s) for the author(s) of this article can be found under https://doi.org/10.1002/adfm.202000815.

DOI: 10.1002/adfm.202000815

Among many members of MXene family, Nb-based materials have been less studied compared to Ti-based MXenes.[19–23] The properties and electrochemical behavior of $Nb_4C_3T_x$ nanosheets as supercapacitors material are still vastly unexplored, which maybe because it was more challenging to delaminate this MXene because of its thicker monolayer. Multilayered $Nb_4C_3T_x$ material exhibits better cycling and rate performance than other MXene materials in lithium-ion batteries,[7] so we anticipate that its delaminated monolayers may perform well. In this paper, we delaminated $Nb_4C_3T_x$ and investigated the electrochemical behavior and capacitance of its flexible freestanding membrane in acidic, alkaline, and neutral electrolytes for the first time. In situ X-ray diffraction (XRD) is used to explore the reaction mechanism in different electrolytes. The chemical and structural stability of $Nb_4C_3T_x$ aqueous suspension and flexible membrane are investigated, which lays a foundation for the energy storage and further application of $Nb_4C_3T_x$.

2. Results and Discussion

Figure 1a shows the XRD pattern of a $Nb_4C_3T_x$ film. From the XRD results, it can be seen that the position of (002) peak is about 5.01°. According to Bragg's equation, this corresponds to a d-spacing of 1.77 nm, which is larger than most previously studied MXenes.[24] For the application of 2D materials in energy storage, larger interlayer space allows faster intercalation and adsorption of ions, and it affects ion diffusion of the electrolyte and charge transport, which controls the electrochemical performance.[25–27] The digital photograph of the flexible film in inset of Figure 1 and Video V1 in the Supporting Information clearly and intuitively demonstrates the flexibility of the film. Scanning electron microscope (SEM) image in Figure 1b shows that almost all the $Nb_4C_3T_x$ sample consists of few layers and single layer, and the size of the flake is about 5 µm. In agreement to SEM image, transmission electron microscope (TEM) results also show a single layer of $Nb_4C_3T_x$, and selective electron diffraction can clearly show the regular hexagonal structure, which is not different from other MXene materials.[24] In addition, the X-ray photoelectron spectroscopy (XPS) confirms the existence of Nb–O bands and Nb–C $3d_{5/2}$ and Nb–C $3d_{3/2}$ on the $Nb_4C_3T_x$ surface, as shown in Figure S1 in the Supporting Information.[28] It indicates that oxygen-containing functional groups generated on the surface may come from the delamination step with TMAOH (tetramethylammonium hydroxide).

In order to better explore the thermal stability of the layered structure of the film for further application, we heated the film to different temperatures, and added flowing nitrogen as a protective gas. XRD results at different temperatures are shown in **Figure 2**a. At 400 °C, the (002) peak shifts obviously to a larger angle, implying that the layered structure gradually stacks or collapses.[29] When the heating temperature reached 800 °C, $Nb_4C_3T_x$ completely transformed to niobium oxide.[30] Thermogravimetric (TG) test result (Figure 2b) shows a mass loss before 125 °C, which is attributed to water desorption. Then the subsequent mass loss comes from the TMAOH molecules, until 400 °C where TMAOH is almost completely removed.[31] The corresponding morphology is shown in SEM images (Figure 2c,d). When the film is heated to 400 °C, it can be seen that the layers are stacked together compactly. When heated to 800 °C, the structure has completely changed, almost no layered morphology can be observed, and granular oxides were formed. In addition, the surface functional groups were also changed, as shown by Raman and FTIR (Fourier transform infrared) spectra after heating to different temperatures (Figure S2, Supporting Information). At 400 °C, the C—F functional groups from hydrogen fluoride (HF) etching process and C—H from TMAOH decreased significantly. However, at 800 °C, the content of oxygen-containing functional groups suddenly increased significantly due to the oxidation of $Nb_4C_3T_x$ to Nb_2O_5, which is consistent with the XRD results.[32,33]

To further investigate the thermal transformation of $Nb_4C_3T_x$, in situ XRD technique was used to record the continuous change of interlayer spacing of flexible membranes during the gradual increase of temperature from room temperature to 500 °C under vacuum conditions, and the test results are shown in **Figure 3**. The full pattern results (3°–65°) in Figure S3 in the Supporting Information show that only (002) peak shifted during the whole heating process. In addition, no other peaks appeared or disappeared, indicating that no phase transition had taken place. The results in the 3°–9° range are shown in Figure 3a. With the increase of temperature, it can be clearly observed that the (002) peak gradually moves to a larger angle, from 5.01° to 5.31°. The corresponding d-spacing of layers varies with temperature, as shown in Figure 3b. Combined with thermogravimetric data, it can be deduced that almost all TMAOH was removed when the temperature was increased to 500 °C, and the spacing between layers decreased from

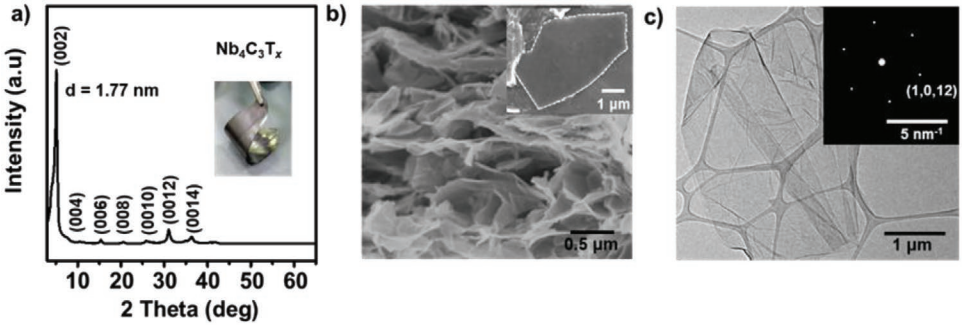

Figure 1. a) XRD pattern of $Nb_4C_3T_x$ film. Inset shows a digital photo. b) SEM image of a $Nb_4C_3T_x$ film in cross-section (inset shows SEM image of a single fkake) and c) TEM image of a $Nb_4C_3T_x$ flake. Inset in (c) shows a selected area electron diffraction pattern.

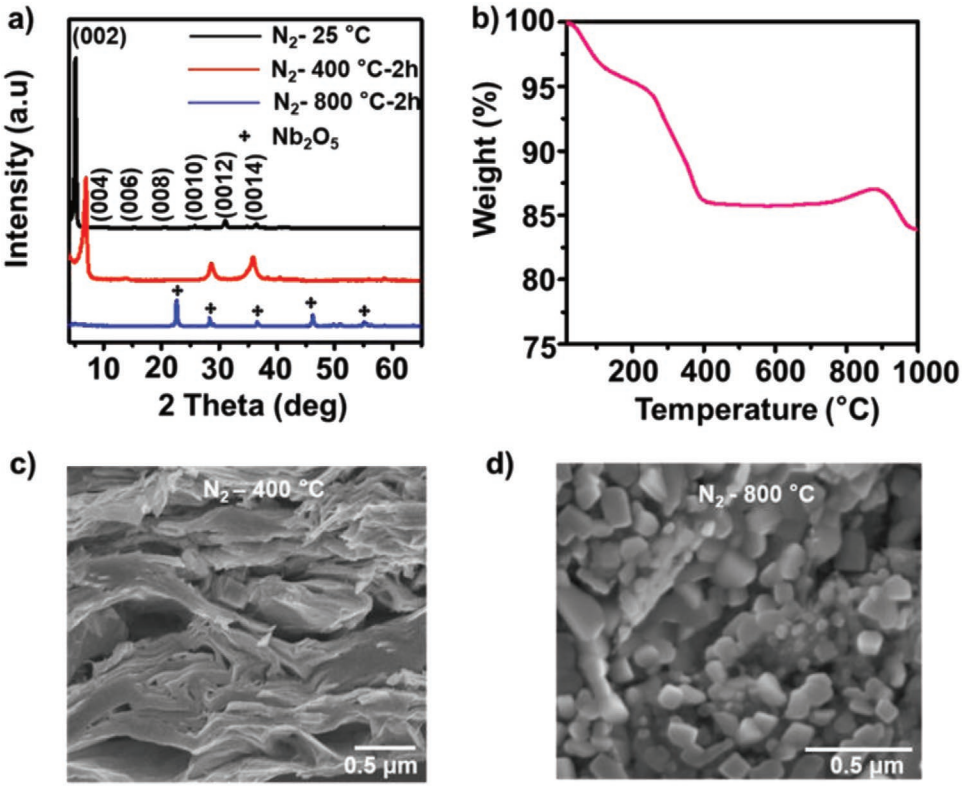

Figure 2. a) XRD patterns of $Nb_4C_3T_x$ films treated at different temperatures in nitrogen. b) Thermogravimetric curve. c,d) SEM images after treatment in nitrogen c) at 400 °C and d) at 800 °C.

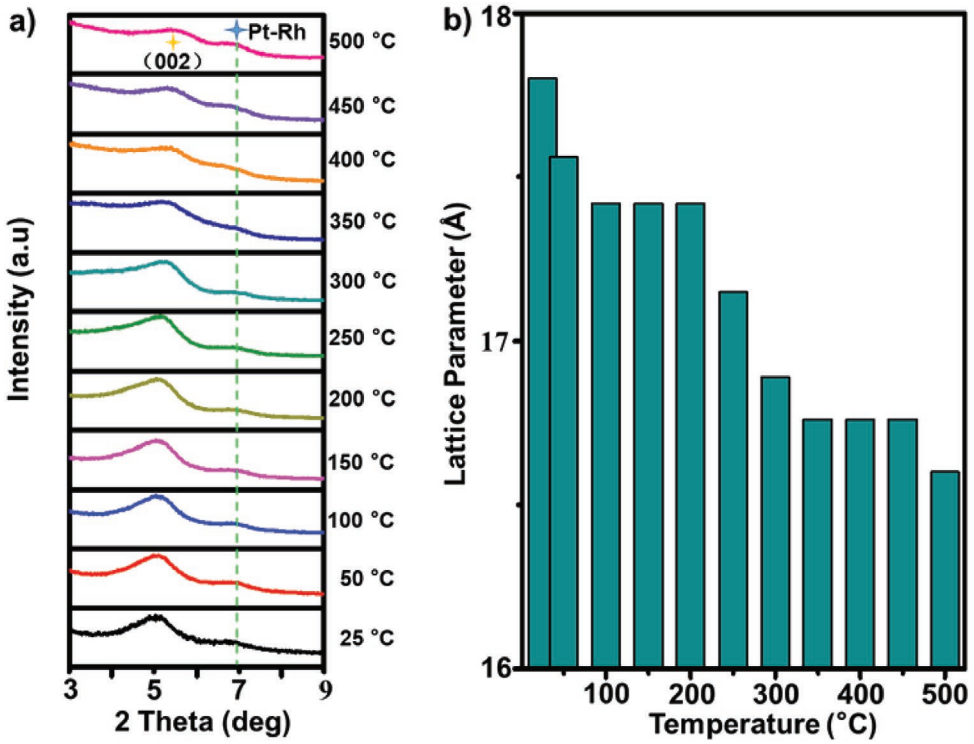

Figure 3. a) In situ XRD patterns of a $Nb_4C_3T_x$ film at different temperatures in vacuum. b) Temperature dependence of *c*-lattice parameter calculated from (002) peak position.

17.7 to 16.6 Å. Therefore, we can conclude that the $Nb_4C_3T_x$ flexible membrane can maintain a d-spacing of 16.6 Å, at least up to 500 °C. Moreover, the conductivity of the flexible membrane $Nb_4C_3T_x$ increased from 5.93×10^3 to 1.01×10^5 S m^{-1} after the removal of TMAOH (heating to 400 °C in N_2 protection and holding for 2 h). But after heating, the film became fragile, and the layers were sintered, which decreased its capacitance in 1 M H_2SO_4, as shown in Figure S4 in the Supporting Information. Therefore, we can conclude that although TMAOH reduces the conductivity of $Nb_4C_3T_x$, its intercalation increases interlayer spacing and is beneficial for achieving high capacitance.

Some MXenes tend to be oxidized in air or aqueous environment,[34] which is detrimental for practical use. It is important to find suitable storage conditions for MXene solution. As-prepared $Nb_4C_3T_x$ suspensions in distilled water (about 0.31 g L^{-1}) were separated and stored in four different conditions, then a part was collected and tested by XRD regularly. The experimental results are shown in **Figure 4**. The first was stored at room temperature (≈26 °C) and the solution became clearer gradually with time (Figure 4a). The XRD results show that after 10 days, the (002) peak became very weak, then when the storage extended to 30 days, the (002) peak disappeared, although there were no niobium oxides peak suggesting oxidation to amorphous Nb oxides or hydroxides. The second was stored in deaerated distilled water produced via bubbling argon through the solution for 15 min and then putting it at room temperature (26 °C). As can be seen from the digital photos in Figure 4b, although the suspension gradually becomes clearer with the prolongation of storage time, the sedimentation rate is slower than that without argon. XRD results show that the intensity of (002) peak decreased, but it could still be detected after 30 days, supporting that argon can prolong the storage time of the material in solution. The third sample was stored as-prepared at lower temperature, about 5 °C, to investigate the effect of the temperature. As shown in Figure 4c, even if stored for 30 days, the solution remained in the state of suspension, and there was no sedimentation. The results of XRD showed that the (002) peak was present and intense when stored at lower temperature for 10 days, but no peak was detected when it was stored for 20 or 30 days. Compared with the storage condition at 26 °C, the lower temperature is beneficial for storage, as the reaction rate is decreased. In conclusion, both the lower temperature and deaeration greatly improve and prolong shelf-life of the $Nb_4C_3T_x$ solution. Figure 4d shows the results after storing under optimized conditions, combining argon bubbling and low temperature. Digital photos confirm that the solution is still colloidal after storing for 30 days. XRD shows that after 30 days, the (002) peak moves to a smaller angle, $2\theta \approx 2.28°$, and the interlayer

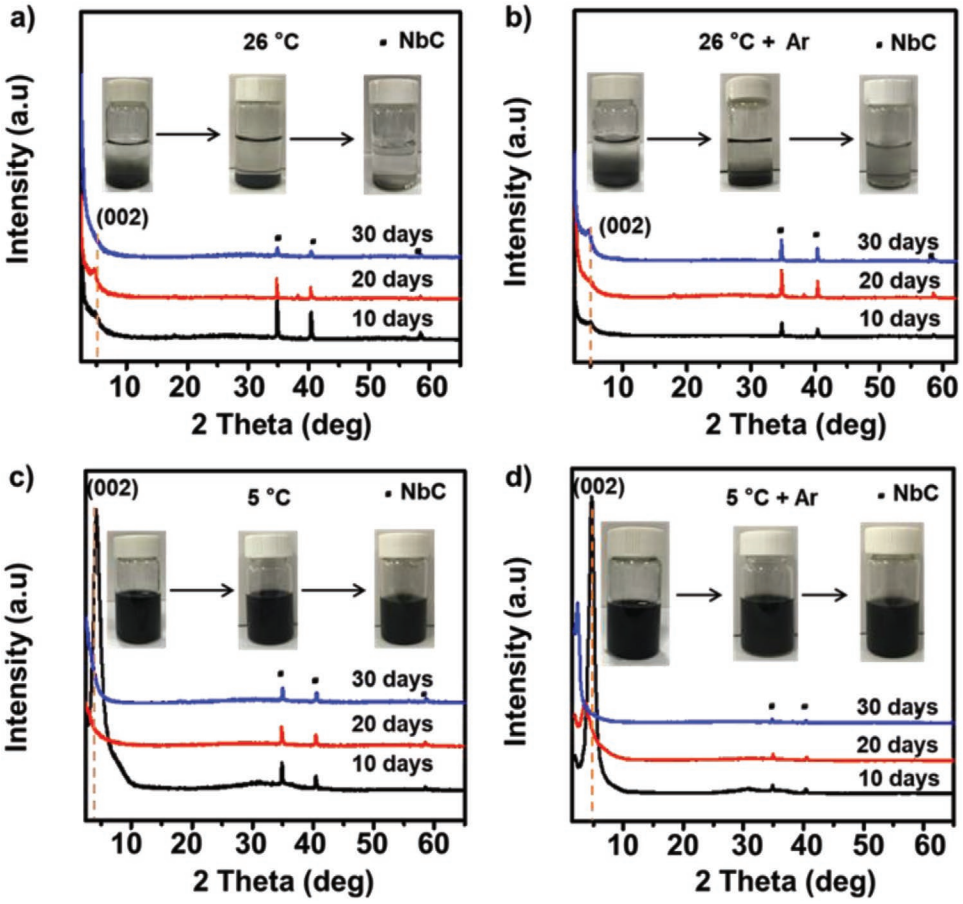

Figure 4. XRD patterns of $Nb_4C_3T_x$ after storing solutions in different conditions. a) As-prepared solution stored at room temperature, b) Ar-filled solution stored at room temperature, c) as-prepared solution stored at 5 °C, and d) Ar-filled solution stored at 5 °C, for 10, 20, and 30 days. Insets are optical images of corresponding solutions.

spacing reaches about 3.87 nm, demonstrating that this storing protocol improves the lifetime of delaminated $Nb_4C_3T_x$ solution. Following the well-studied oxidation of $Ti_3C_2T_x$, which leads to the formation of TiO_2, free carbon, and methane, we propose the decomposition reactions in water may follow the same path[34,35]

$$Nb_4C_3O_2 + (4x-2)H_2O = 4NbO_x + 3C + (4x-2)H_2 \quad (1)$$

$$Nb_4C_3O_2 + 6H_2O = 4NbO_2 + 3CH_4 \quad (2)$$

Low-temperature storage and deaeration of water can decrease the reaction rate, which is beneficial for prolonging the lifetime of MXene suspension in water. Transfer to other solvent, such as isopropanol, has also been suggested.[35]

Figure 5 shows the electrochemical performance of $Nb_4C_3T_x$ flexible film in different electrolytes. Figure 5a–c corresponds to the cyclic voltammograms (CVs) in three different electrolytes: 1 м H_2SO_4, 1 м KOH, and 1 м $MgSO_4$, respectively. Comparing the curves in the three different electrolytes, only one pair of redox peaks appeared in 1 м KOH at about −0.96 and −0.7 V versus Ag. Unlike KOH, there is a pair of broad redox peaks at about −0.44 and −0.5 V versus Ag in 1 м H_2SO_4 at the scan rate of 5 mV s^{-1}. However, in 1 м $MgSO_4$, there are almost no peaks distinguishable and the rate performance is poor. Figure 5d summarizes the volumetric capacitance of $Nb_4C_3T_x$ in three electrolytes at different scan rates. At the scan rate of 5 mV s^{-1}, the volumetric capacitance in 1 м H_2SO_4, 1 м KOH, and 1 м $MgSO_4$ is 1075, 687, and 506 F cm^{-3} (gravimetric capacitances are shown in Figure S5a, Supporting Information), respectively, which is higher than most of MXenes and MXene-based hybrid electrodes.[36–38] However, at higher scan rates, the CVs appear more resistive compared to $Ti_3C_2T_x$ MXene,[15] which might be due to the larger nanosheet size and lower electronic conductivity of $Nb_4C_3T_x$, which is detrimental to high rate capability.[39] This could theoretically be improved by decreasing the flake's size, using conductive additive-preventing restacking of 2D sheets, or tuning the electrode architecture, as it was done for $Ti_3C_2T_x$.[40] Furthermore, EIS (electrochemical impedance spectra) can directly display ion and charge transfer dynamics, showing series resistance, charge transfer resistance, and diffusion of ions within electrode materials. Comparing the Nyquist plots of $Nb_4C_3T_x$ in three different aqueous electrolytes (Figure S5b, Supporting Information), we concluded that MXene film in 1 м $MgSO_4$ shows the largest series resistance (intercept of semicircle on the real impedance axis), and the electrode in 1 м H_2SO_4 shows the lowest charge transfer resistance (smallest semicircle) and fastest diffusion of ions (steepest slope of the Nyquist plot in the low-frequency range).[41] Potassium ions fall between protons and magnesium ions. Because of the smaller radius of H^+, it is easier for protons to migrate in the MXene interlayer space, which is consistent with the electrochemical performance. Lifetime is an important indicator of capacitor. When testing the cycle life of $Nb_4C_3T_x$ at the current density of 2 A g^{-1}, it was found that the material exhibited different capacitance retention in the three different electrolytes. After 5000 cycles, in 1 м H_2SO_4 (Figure 5e), the capacity retention is about 76%. From the charge–discharge curves (Figure 5f), a large resistance is observed, which results in irreversible capacity

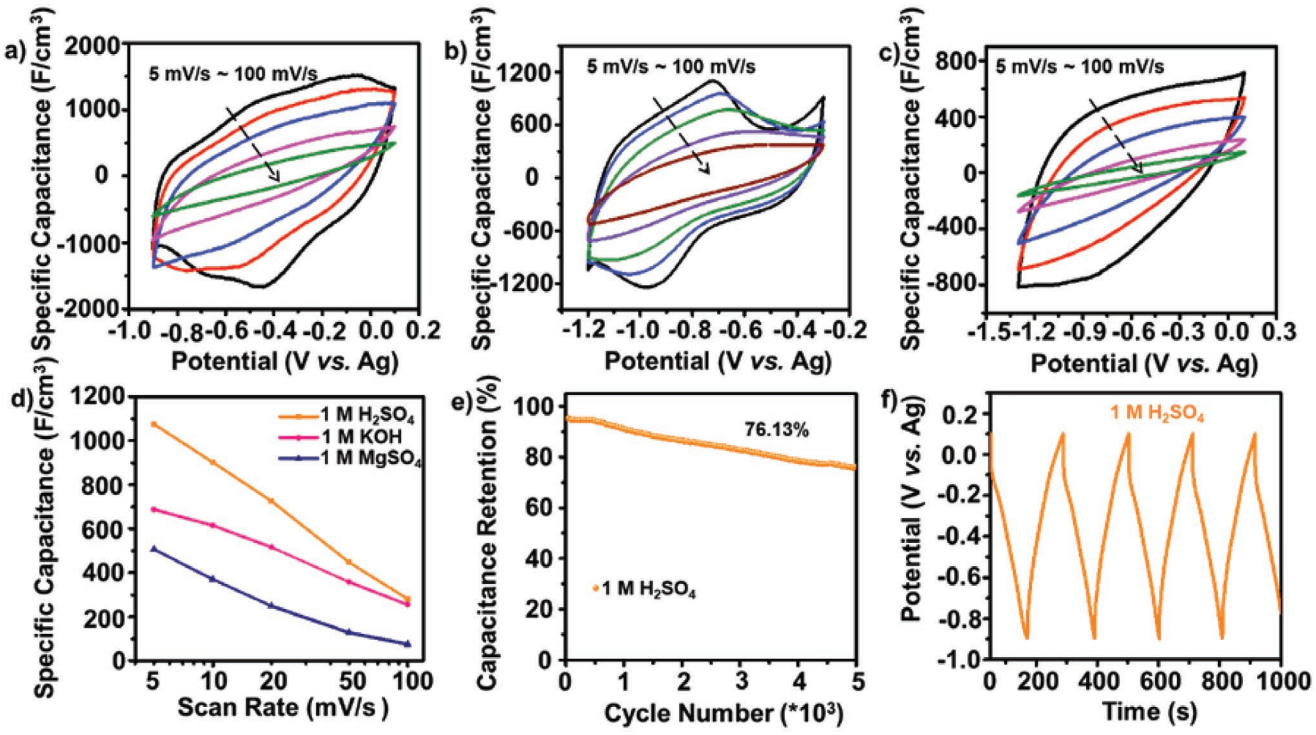

Figure 5. Electrochemical performance of $Nb_4C_3T_x$ film. CVs at different scan rates in a) 1 м H_2SO_4, b) 1 м KOH, and c) 1 м $MgSO_4$. d) Specific capacitance measured from corresponding CVs. e) Cycle lives measured from galvanostatic charge–discharge at 2 A g^{-1} and f) profiles in 1 м H_2SO_4.

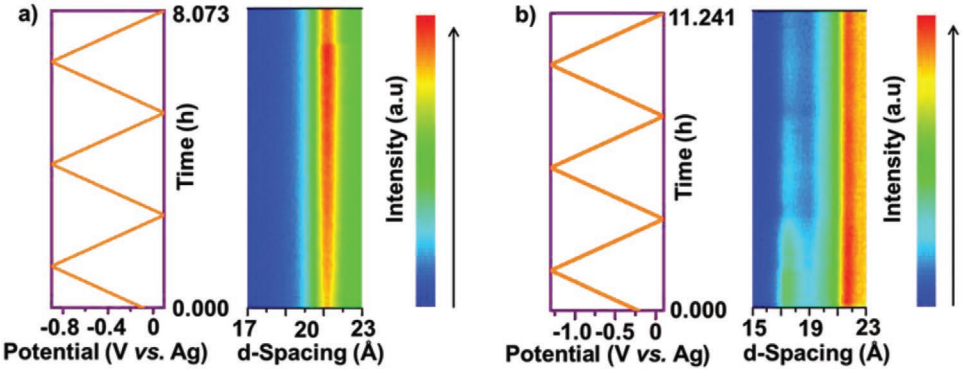

Figure 6. In situ XRD patterns during electrochemical cycles in a) 1 M H_2SO_4 and b) 1 M $MgSO_4$.

loss in the process of charge–discharge. This may be due to the use of TMAOH as a delamination agent in the process of material preparation, which reduces the electronic conductivity of the material. In 1 M KOH solution, after 1000 cycles, the capacity retention is only 49% (Figure S6, Supporting Information). Because Nb ions were detected by inductive plasma spectroscopy after 1000 cycles, it can be deduced that $Nb_4C_3T_x$ dissolves gradually in KOH solution during cycling. The mechanism of dissolution needs to be studied in further work. In 1 M $MgSO_4$, after 5000 cycles, the capacitance retention is about 58% (Figure S7, Supporting Information). No dissolution was observed. By comparing XRD before and after the cycling (Figure S8a,b, Supporting Information), we found that, after cycling, the peak (002) of $Nb_4C_3T_x$ shifted to a larger angle, indicating that the interlayer spacing decreased, suggesting extraction of TMAOH along with the collapse and restacking of layers as the main reason for capacitance loss. SEM images (Figure S8c,d, Supporting Information) also suggest that interlayer distance was decreased.

In order to explore the reaction mechanism of $Nb_4C_3T_x$ in 1 M H_2SO_4 and 1 M $MgSO_4$, we carried out in situ XRD tests (as $Nb_4C_3T_x$ dissolves in KOH, in situ XRD characterization in this electrolyte was not prioritized). **Figure 6**a is the relationship between d-spacing (2θ = 3.8°–5.19°) and time in 1 M H_2SO_4. During the three charge–discharge cycles, (002) peak did not move significantly. We believe that this is because the interlayer spacing (21 Å) is large enough to accommodate the intercalation of H^+ without any lattice expansion. The same phenomenon also occurs in 1 M $MgSO_4$ solution (Figure 6b, 2θ = 3.8°–5.8°), with the interlayer spacing as high as 21.5 Å. However, because the radius of Mg^{2+} ions is larger than that of H^+, after thousands of cycles, they can remove TMAOH, resulting in the lower capacitance retention. This mechanism is different from $Ti_3C_2T_x$, where the smaller interlayer distance is observed to change during each cycle of surface protonation/deprotonation.[42,43]

3. Conclusions

Colloidal solutions and free-standing films of $Nb_4C_3T_x$ were prepared by delamination with the help of TMAOH. The $Nb_4C_3T_x$ interlayer spacing in the film reached 1.77 nm, the large layer distance is beneficial to electrochemical performance. We have shown that the deaerated $Nb_4C_3T_x$ solution can be stored for more than 30 days, when refrigerated. Importantly, the $Nb_4C_3T_x$ has shown promising electrochemical performance in supercapacitors, especially in 1 M H_2SO_4 electrolyte. At the scan rate of 5 mV s^{-1}, the volumetric capacitances of $Nb_4C_3T_x$ in 1 M H_2SO_4, 1 M KOH, and 1 M $MgSO_4$ are 1075, 687, and 506 F cm^{-3}, respectively. The large interlayer spacing can accommodate the intercalation/deintercalation of ions without destroying the layered structure of MXene electrode. Among many members of the MXene family, $Nb_4C_3T_x$ shows obvious advantages in volumetric capacitance, and is suitable for wearable and portable devices.

4. Experimental Section

Preparation of $Nb_4C_3T_x$ Film: Commercial powders of niobium (99.9% metals basis, 325 mesh), aluminum (99.8% purity, 300 mesh), and carbon black (99% purity, 300 mesh) were used as precursors for the synthesis of Nb_4AlC_3. The synthetic method was the same as previously reported.[7] During etching step, 0.4 g Nb_4AlC_3 powder was added to 30 mL HF solution (49% HF, Aladdin) under stirring at room temperature (20–25 °C) for 140 h. This acidic mixture was washed by deionized water (DI H_2O) followed by centrifugation (5000 rpm, 6 min per cycle). After each centrifugation cycle, the supernatant was discarded and the sediment was dispersed in DI H_2O until neutral pH (≈7) was reached. To delaminate the $Nb_4C_3T_x$, 1 mL of organic base tetramethylammonium hydroxide (TMAOH 25% in H_2O, Aladdin, China) was mixed with 9 mL DI H_2O, then $Nb_4C_3T_x$ was added and shaken for 15 min at room temperature. The excess TMAOH was separated from the product by repeated centrifugation at 3500 rpm. The resulting wet sediment formed a clay-like paste that could be rolled between water-permeable membranes to produce flexible, freestanding films. The as-prepared $Nb_4C_3T_x$ films were heated at a heating rate of 5 °C min^{-1} to 400 or 800 °C for 2 h in a tube furnace under nitrogen flow as a protective gas, and then cooled down to room temperature for further study.

Characterization: An X-ray diffractometer (XRD, Bruker D8) with Cu Kα radiation (λ = 0.15406 nm) was used to characterize $Nb_4C_3T_x$ structure and composition both ex situ and in situ. The in situ XRD study of heating to different temperatures in vacuum was carried out in a 2θ range of 3°–65° with a step width of 0.019°. The samples were placed onto a platinum-rhodium substrate. When the specified temperature was reached, it was maintained for 5 min before recording the pattern (≈15 min).

An SEM (JSM-6700F) and a TEM (JEM-2200FS) were used to observe the morphology and microstructure of the samples. The TG analysis was carried out using an SDT-Q600 thermal gravimetric analyzer in N_2 flow with a heating rate of 10 °C min^{-1} from room temperature to 1000 °C.

XPS (ESCALAB) analysis was conducted using a Mg-Kα light source. FTIR (BRUKER, VERTEX 70) was used to examine the presence of functional groups on the surface of $Nb_4C_3T_x$. Raman spectroscopy was carried out using a HORIBA HR Evolution Raman spectrometer with a 532 nm diode-pumped solid-state laser.

Preparation of Electrode and Electrochemical Measurements: $Nb_4C_3T_x$ films were punched into 6 mm diameter disks with mass loadings about 3.75 g cm^{-3} and used directly as binder-free electrodes. The electrochemical performance was investigated using a VMP3 potentiostat (Biologic, S.A.) with three-electrode Swagelok cells, delaminated $Nb_4C_3T_x$ film was the working electrode, overcapacitive activated carbon was the counter electrode, cellulose membrane was the separator, and Ag wire was used as the reference electrode. 1 M H_2SO_4, 1 M KOH, and 1 M $MgSO_4$ solutions were used as electrolytes. EIS was also performed with the VSP instrument in the frequency range of 10 mHz to 200 kHz.

Supporting Information

Supporting Information is available from the Wiley Online Library or from the author.

Acknowledgements

This work was financially supported by the Science & Technology Department of Jilin Province (nos. 20180101199JC, 20180101204JC) and Jilin Province/Jilin University Co-construction Project-Funds for New Materials (SXGJSF2017-3).

Conflict of Interest

The authors declare no conflict of interest.

Keywords

flexible devices, MXenes, niobium carbide, supercapacitors

Received: January 28, 2020
Revised: March 4, 2020
Published online:

[1] W. F. Wei, X. W. Cui, W. X. Chen, D. G. Ivey, *Chem. Soc. Rev.* **2011**, *40*, 1697.
[2] L. L. Zhang, X. S. Zhao, *Chem. Soc. Rev.* **2009**, *38*, 2520.
[3] C. G. Liu, Z. N. Yu, D. Neff, A. Zhamu, B. Z. Jang, *Nano Lett.* **2010**, *10*, 4863.
[4] X. Liang, A. Garsuch, L. F. Nazar, *Angew. Chem., Int. Ed.* **2015**, *54*, 3907.
[5] J. M. Li, N. Kurra, M. Seredych, X. Meng, H. Z. Wang, Y. Gogotsi, *Nano Energy* **2019**, *56*, 151.
[6] Q. M. Shan, X. P. Mu, M. Alhabeb, C. E. Shuck, D. Pang, X. Zhao, X. F. Chu, Y. J. Wei, F. Du, G. Chen, Y. Gogotsi, Y. Gao, Y. Dall'Agnese, *Electrochem. Commun.* **2018**, *96*, 103.
[7] S. S. Zhao, X. Meng, K. Zhu, F. Du, G. Chen, Y. J. Wei, Y. Gogotsi, Y. Gao, *Energy Storage Mater.* **2017**, *8*, 42.
[8] O. Mashtalir, M. R. Lukatskaya, M. Q. Zhao, M. W. Barsoum, Y. Gogotsi, *Adv. Mater.* **2015**, *27*, 3501.
[9] J. Ran, G. Gao, F. T. Li, T. Y. Ma, A. J. Du, S. Z. Qiao, *Nat. Commun.* **2017**, *8*, 13907.
[10] H. Wang, R. Peng, Z. D. Hood, M. Naguib, S. P. Adhikari, Z. L. Wu, *ChemSusChem* **2016**, *9*, 1490.
[11] L. Yang, Y. Dall'Agnese, K. Hantanasirisakul, C. E. Shuck, K. Maleski, M. Alhabeb, G. Chen, Y. Gao, Y. Sanehira, A. K. Jena, L. Shen, C. X. Dall'Agnese, X. F. Wang, Y. Gogotsi, T. Miyasaka, *J. Mater. Chem. A* **2019**, *7*, 5635.
[12] Q. Zhang, J. Teng, G. D. Zou, Q. M. Peng, Q. Du, T. F. Jiao, J. Y. Xiang, *Nanoscale* **2016**, *8*, 7085.
[13] B. M. Jun, S. Kim, J. Y. Heo, C. M. Park, N. Her, M. Jang, Y. Huang, J. H. Han, Y. Yoon, *Nano Res.* **2019**, *12*, 471.
[14] M. Ghidiu, M. R. Lukatskaya, M. Q. Zhao, Y. Gogotsi, M. W. Barsoum, *Nature* **2014**, *516*, 78.
[15] M. R. Lukatskaya, S. Kota, Z. F. Lin, M. Q. Zhao, N. Shpigel, M. D. Levi, J. Halim, P. L. Taberna, M. W. Barsoum, P. Simon, Y. Gogotsi, *Nat. Energy* **2017**, *2*, 17105.
[16] P. T. Yan, R. J. Zhang, J. Jia, C. Wu, A. G. Zhou, J. Xu, X. S. Zhang, *J. Power Sources* **2015**, *284*, 38.
[17] Z. Ling, C. E. Ren, M. Q. Zhao, J. Yang, J. M. Giammarco, J. S. Qiu, M. W. Barsoum, Y. Gogotsi, *Proc. Natl. Acad. Sci. USA* **2014**, *111*, 16676.
[18] Q. Gao, J. Come, M. Naguib, S. Jesse, Y. Gogotsi, N. Balke, *Faraday Discuss.* **2017**, *199*, 393.
[19] C. F. Hu, F. Z. Li, J. Zhang, J. M. Wang, J. Y. Wang, Y. C. Zhou, *Scr. Mater.* **2007**, *57*, 893.
[20] Y. Xin, Y. X. Yu, *Mater. Des.* **2017**, *130*, 512.
[21] M. Ghidiu, M. Naguib, C. Shi, O. Mashtalir, L. M. Pan, B. Zhang, J. Yang, Y. Gogotsi, S. J. L. Billingebd, M. W. Barsoum, *Chem. Commun.* **2014**, *50*, 9517.
[22] S. S. Zhao, Y. Dall'Agnese, X. F. Chu, X. Zhao, Y. Gogotsi, Y. Gao, *ACS Energy Lett.* **2019**, *4*, 2452.
[23] A. Lipatov, M. Alhabed, H. D. Lu, S. S. Zhao, M. J. Loes, N. S. Vorobeva, Y. Dall'Agnese, Y. Gao, A. Gruverman, Y. Gogotsi, *Adv. Electron. Mater.* **2020**, *6*, 1901382.
[24] J. B. Pang, R. G. Mendes, A. Bachmatiuk, L. Zhao, H. K. Ta, T. Gemming, H. Liu, Z. F. Liu, M. H. Rummeli, *Chem. Soc. Rev.* **2019**, *48*, 72.
[25] Z. H. Pan, F. Cao, X. Hu, X. H. Ji, *J. Mater. Chem. A* **2019**, *7*, 8984.
[26] J. M. Luo, W. K. Zhang, H. D. Yuan, C. B. Jin, L. Y. Zhang, H. Huang, C. Liang, Y. Xia, J. Zhang, Y. P. Gan, X. Y. Tao, *ACS Nano* **2017**, *11*, 2459.
[27] W. L. Wu, D. Wei, J. F. Zhu, D. J. Niu, F. Wang, L. Wang, L. Q. Yang, P. P. Yang, C. W. Wang, *Ceram. Int.* **2019**, *45*, 7328.
[28] J. Yang, M. Naguib, M. Ghidiu, L. M. Pan, J. Gu, J. Nanda, J. Halim, Y. Gogotsi, M. W. Barsoum, *J. Am. Ceram. Soc.* **2016**, *99*, 660.
[29] R. B. Rakhi, B. Ahmed, M. N. Hedhili, D. H. Anjum, H. N. Alshareef, *Chem. Mater.* **2015**, *27*, 5314.
[30] C. F. Zhang, S. J. Kim, M. Ghidiu, M. Q. Zhao, M. W. Barsoum, V. Nicolosi, Y. Gogotsi, *Adv. Funct. Mater.* **2016**, *26*, 4143.
[31] K. Hantanasirisakul, M. Alhabeb, A. Lipatov, K. Maleski, B. Anasori, P. Salles, C. Ieosakulrat, P. Pakawatpanurut, A. Sinitskii, S. J. May, Y. Gogotsi, *Chem. Mater.* **2019**, *31*, 2941.
[32] E. E. Ibrahim, D. M. Chipara, R. Thapa, K. Lozano, M. R. Chipara, *J. Nanomater.* **2012**, 2012, 793084.
[33] A. Pawlicka, M. Atik, M. A. Aegerter, *Thin Solid Films* **1997**, *301*, 236.
[34] C. F. Zhang, S. Pinilla, N. McEvoy, C. P. Cullen, B. Anasori, E. Long, S. H. Park, A. Seral-Ascaso, A. Shmeliov, D. Krishnan, C. Morant, X. H. Liu, G. S. Duesberg, Y. Gogotsi, V. Nicolosi, *Chem. Mater.* **2017**, *29*, 4848.
[35] S. H. Huang, V. N. Mochalin, *Inorg. Chem.* **2019**, *58*, 1958.
[36] M. Q. Zhao, C. E. Ren, Z. Ling, M. R. Lukatskaya, C. F. Zhang, K. L. Aken, M. W. Barsoum, Y. Gogotsi, *Adv. Mater.* **2015**, *27*, 339.

[37] J. Yan, C. E. Ren, K. Maleski, C. B. Hatter, B. Anasori, P. Urbankowski, A. Sarycheva, Y. Gogotsi, *Adv. Funct. Mater.* **2017**, *27*, 1701264.
[38] M. S. Zhu, Y. Huang, Q. H. Deng, J. Zhou, Z. X. Pei, Q. Xue, Y. Huang, Z. F. Wang, H. F. Li, Q. Huang, C. Y. Zhi, *Adv. Energy Mater.* **2016**, *6*, 1600969.
[39] B. Anasori, M. R. Lukatskaya, Y. Gogotsi, *Nat. Rev. Mater.* **2017**, *2*, 16098.
[40] X. Zhang, Z. H. Zhang, Z. Zhou, *J. Energy Chem.* **2018**, *27*, 73.
[41] M. G. Jung, G. S. Gund, Y. Gogotsi, H. S. Park, *Batteries Supercaps* **2020**, *3*, 354.
[42] X. P. Mu, D. S. Wang, F. Du, G. Chen, C. Z. Wang, Y. J. Wei, Y. Gogotsi, Y. Gao, Y. Dall'Agnese, *Adv. Funct. Mater.* **2019**, *29*, 1902953.
[43] X. Zhao, C. X. Dall'Agnese, X. F. Chu, S. S. Zhao, G. Chen, Y. Gogotsi, Y. Gao, Y. Dall'Agnese, *ChemSusChem* **2019**, *12*, 4480.